Proceedings of the ASME 2021
International Mechanical Engineering Congress and Exposition
IMECE2021
November 1-5, 2021, Virtual, Online

IMECE2021-72026

CHEMICAL STRUCTURE ANALYSIS OF CARBON-DOPED SILICON OXIDE THIN FILMS BY PLASMA-ENHANCED CHEMICAL VAPOR DEPOSITION OF TETRAKIS(TRIMETHYLSILYLOXY)SILANE PRECURSOR

Jacob Comeaux
Department of Mechanical Engineering
University of Louisiana at Lafayette
Lafayette, LA

William B. Wirth
Department of Mechanical Engineering
University of Louisiana at Lafayette
Lafayette, LA

Justin Courville
Department of Mechanical Engineering
University of Louisiana at Lafayette
Lafayette, LA

Lingyiqian Luo
Department of Chemistry
University of Louisiana at Lafayette
Lafayette, LA

Hui Yan
Department of Chemistry
University of Louisiana at Lafayette
Lafayette, LA

Seonhee Jang
Department of Mechanical Engineering
University of Louisiana at Lafayette
Lafayette, LA

ABSTRACT

Carbon-doped silicon oxide (CDO) thin films as low dielectric constant materials were deposited on both n-type silicon (Si) (100) and indium tin oxide coated polyethylene naphthalate (ITO/PEN) substrates, using the plasma-enhanced chemical vapor deposition of tetrakis(trimethylsilyoxy)silane (TTMSS) precursor. Chemical structures of the CDO films were analyzed by using FTIR (Fourier transformation infrared) spectroscopy and XPS (X-ray photoelectron spectroscopy). The chemical bonds related with hydrocarbon and Si–O were the main characteristics of the CDO films. The prominent peaks from the FTIR spectra included Si–O–Si stretching, Si–CH_3 bending, Si–$(CH_3)_x$ stretching, and CH_x stretching modes. XPS spectra composed of the O1s, C1s, and Si2p electron orbitals were used to quantitatively analyze the elemental composition of the CDO films. The growth mechanisms of CDO films were dependent on the substrate type. For the ITO/PEN substrate, the lack of Si atoms on the ITO surface made difficulty in forming initial Si–O bonds, resulting in insufficient Si–O–Si structure. In comparison, the CDO films could grow easily on Si substrates due to pre-existing Si–O bonds on the surface. The chemical structures of the CDO films are expected to affect electrical and mechanical performances.

Keywords: Carbon-doped silicon oxide, low dielectric constant, plasma-enhanced chemical vapor deposition, tetrakis(trimethylsilyoxy)silane

NOMENCLATURE

α	alpha
Ω	ohm

1. INTRODUCTION

Continuous downscaling and performance improvement of the next-generation electronic devices such as logic and memory devices, displays, sensors, and solar cells require new materials and new fabrication schemes. In advanced interconnects, resistive-capacitive (RC) delay induced by the product of the resistance of the metal lines and their inter-capacitance becomes important because it can be a significant obstacle to continued downward scaling of devices [1-4]. In order to reduce the resistance in RC delay, aluminum (Al) was replaced by copper (Cu) with lower resistivity for metal lines. To decrease capacitance, the conventional silicon oxide (SiO_2, k~4.2) inter-metal dielectric (IMD) was replaced by the materials with lower dielectric constant k, so called "low-k" materials. As low-k materials, fluorine (F)-doped materials including F-doped oxide

(SiOF) and F-doped amorphous carbon (a-C:F) or carbon (C)-doped oxide (also called SiCOH). The carbon-doped oxide, consisting of silicon (Si), carbon (C), oxygen (O), and hydrogen (H), shows its *k* values below 2.5 [5-8]. On the other hand, there has been increasing demand for the development of flexible electronic devices on polymer substrates with high flexibility and conformability. For the fabrication of flexible devices, the materials should have good compatibility with various flexible substrates.

Most current carbon-doped oxide (CDO) thin films are formed via plasma-enhanced chemical vapor deposition (PECVD) [9-14]. It should be noted that the chemical structures of CDO thin films are strongly related to their mechanical and electrical properties [15-17]. Thus, chemical properties of CDO thin films as low-*k* materials should be understood for a wide range of the applications in electronic devices fabrication.

In this study, a precursor of tetrakis(trimethylsilyloxy)silane (TTMSS, $C_{12}H_{36}O_4Si_5$) was used to deposit the CDO thin films using PECVD method. Two types of substrates, an n-type Si (100) and indium tin oxide coated polyethylene naphthalate (ITO/PEN) substrates were employed. Fourier transformation infrared (FTIR) spectroscopy and X-ray photoelectron spectroscopy (XPS) were used to study the chemical structures of the CDO films at varying plasma powers. Spectra from FTIR and XPS were analyzed through the assigning of peak values and the calculation of peak area ratios, aiding in the identification of various chemical bond configurations resulting in the formation of various chemical compounds in the CDO thin-films. The chemical structures were compared depending on the substrate type.

2. MATERIALS AND METHODS

As low-*k* materials, CDO thin films were deposited using the PECVD of TTMSS (Sigma Aldrich, 97% purity) precursor. Figure 1 shows the molecular schematic of TTMSS precursor. TTMSS has a cross shape structure made up of a central Si atom with four oxygen atoms bonded to it. Attached to each oxygen atom is a second silicon atom bonded to three CH_3 groups. For this experiment, 4-inch rigid Si wafers and flexible substrates were used: phosphorus-doped n-type Si (100) with a resistivity of 1-10 Ω·cm and indium tin oxide coated polyethylene naphthalate (ITO/PEN) substrates with a sheet resistance of 12 Ω/square. Ultrasonic cleaning in acetone and ethanol, each for five minutes, and three deionized water rinses were used to clean the Si substates. The ITO/PEN substates included a protective thin film that was removed before deposition. To vaporize the precursor molecules, the bubbler containing TTMSS precursor was heated to 85 °C. Ultra-high purity argon (Ar, 99.999%) was used as the carrier gas to introduce the TTMSS vapors into the chamber through the shower head. The distance between substrate holder and shower head was 20 mm. The substate holder was kept at room temperature. Before deposition, three minutes of Ar plasma was conducted at 50 W with a radio frequency (RF) of 13.56 MHz to clean and activate the Si and ITO/PEN substrates. Base pressure was then reached at 4×10^{-3} Torr (0.53 Pa) after vacuuming the chamber. Gas flow was maintained at 18 sccm and 30 Torr (4.0 kPa) using a mass flow controller (MFC) and pressure flow controller (PFC), respectively. The operating pressure during deposition was kept at 200 mTorr (26.7 Pa). RF plasma power was varied between 20 and 100 W.

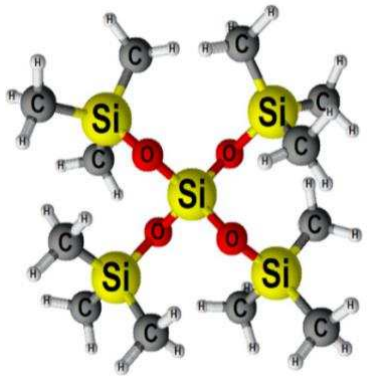

FIGURE 1: CHEMICAL STRUCTURE OF TTMSS PRECURSOR.

Chemical analysis was performed on both Si and ITO/PEN samples using FTIR and XPS. The FTIR systems (Invenio-S, Bruker for Si and Cary 630, Agilent Tech for ITO/PEN, both ATR mode) were used to analyze chemical bonds in the thin films by detection of the various bond vibration modes with wavenumbers in the range of 4000-600 cm^{-1}. The XPS system (ESCA 2SR, ScientaOmicron) was used to analyze the various element peaks and corresponding binding energy with a survey scan (0-1200 eV), scanning step of 0.1 eV, and with a mono Al Kα X-ray source (1486.6 eV). Additionally, atomic concentrations were calculated for each sample using a high-resolution scan of predominant peaks. Before scanning, surface contaminations were removed by Ar sputtering of Si and ITO/PEN samples for 3 min and 5 min, respectively. Sputtering times were determined via a depth profiling experiment in which data was acquired and analyzed at various sputtering times. In the XPS analysis, a carbon correction was used based on C1s (C–C/C–H, 284.8 eV). OriginPro and CasaXPS software were used with Gaussian peak fitting to deconvolute the peaks of the spectra obtained from FTIR and XPS analysis, respectively.

3. RESULTS AND DISCUSSION

3.1 CDO Thin Films Deposited on Si Substates

FTIR analysis was used to study the effects of varying plasma power on the chemical bonding structure of the CDO thin films. Figure 2 presents the FTIR spectra over wavenumbers from 4000 to 600 cm^{-1} for varying plasma powers from 20 to 100 W. The peak assignments in the spectra allowed to identify the chemical bond structures. Hydrocarbon and Si–O-related bonds were the main features of the CDO films. The two prominent

peaks at 1200-900 cm^{-1} and 1300-1200 cm^{-1} were associated with Si–O–Si stretching and Si–CH_3 bending modes, respectively. Additionally, peaks were detected at 950-650 cm^{-1} and 3000-2800 cm^{-1} corresponding to Si–$(CH_3)_x$ stretching and CH_x stretching modes, respectively.

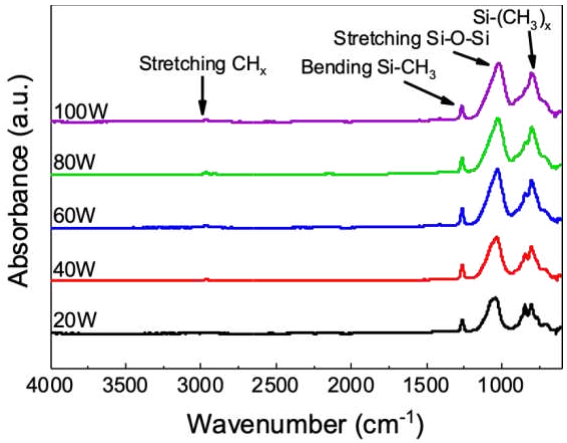

FIGURE 2: FTIR SPECTRA OF CDO THIN FILMS ON Si SUBSTRATE AT VARYING PLASMA POWERS.

Figures 3(a) and (b) present Si–O–Si stretching modes between 1200-900 cm^{-1} plotted at varying plasma powers of 20-100 W and its deconvoluted peaks at the plasma power of 20 W, respectively. As the plasma power increased from 20 to 60 W, the peak intensity of Si–O–Si increased. With further increase in the plasma power to 100 W, the intensity decreased. The peaks were deconvoluted into three components corresponding to cage (1023 cm^{-1}), network (1063 cm^{-1}), and suboxide (1135 cm^{-1}) bonding configurations based on the Si–O–Si bonding angle [18-20]. The cage structure is associated with a large bond angle around 150° for Si–O–Si bonds. The network structure has a smaller stretching angle of Si–O–Si bonds compared to the cage structure. Various silicon suboxide structures include long polymer chains, ring structures, or random structures. It was known that the fraction of cage, network, and suboxide structures contributes to the formation of porosity and thus dielectric constant and mechanical strength. Similarly, in Figure 3(c), FTIR spectra for Si–CH_3 bending modes between 1300-1200 cm^{-1} were plotted at varying plasma powers of 20-100 W and deconvoluted as shown for the plasma power of 20 W in Figure 3(d). As the plasma power increased from 20 to 60 W, the peak intensity of Si–CH_3 increased and then decreased with an increase of the plasma power to 100 W. Si–CH_3 peaks were deconvoluted into an M-Group (1254 cm^{-1}), D-Group (1262 cm^{-1}), and T-Group (1273 cm^{-1}). The M-, D-, and T-groups corresponded to $OSi–(CH_3)_3$, $O_2Si–(CH_3)_2$, and $O_3Si–CH_3$, respectively, containing a single silicon atom linked to varying numbers of methyl groups and oxygen atoms.

Figures 4(a) and (b) show Si–$(CH_3)_x$ stretching modes in the 950 and 650 cm^{-1} range at varying plasma powers of 20-100 W and its deconvoluted peaks at the plasma power of 20 W, respectively. The peaks were assigned into H–SiO_3, H–SiO_2Si, $Si(CH_3)_1$, $Si(CH_3)_2$, $Si(CH_3)_3$, and Si–O–Si bonding. Figures 4(c) and (d) present CH_x stretching modes between 3000-2800 cm^{-1} plotted for varying plasma powers of 20-100 W and its deconvoluted peaks at the plasma power of 20 W, respectively. The CH_x peaks were deconvoluted into two peaks corresponding to asymmetric CH_3 and symmetric CH_3 bonding. Herein, the details of these four absorption bands are presented based on the analyses of the peak area ratios.

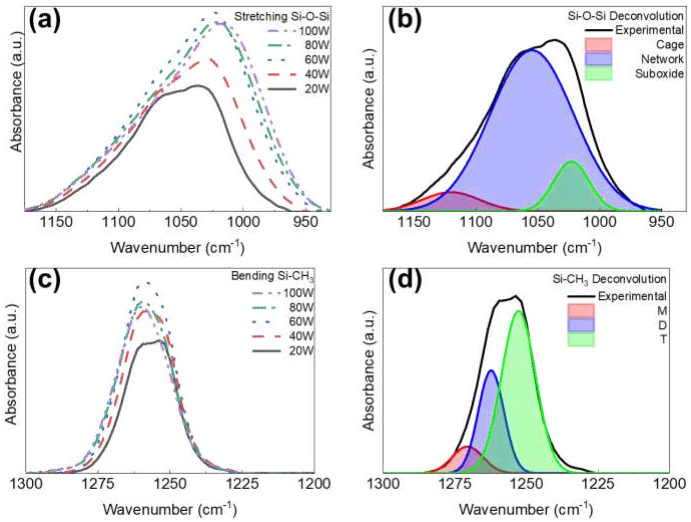

FIGURE 3: (a) FTIR ABSORPTION BAND OF Si–O–Si (900-1200 CM^{-1}) OF CDO FILMS ON Si SUBSTATE AT VARYING PLASMA POWERS, (b) DECONVOLUTED Si–O–Si PEAK AT 20 W, (c) FTIR ABSORPTION BAND OF Si–CH_3 (1225-1300 CM^{-1}) AT VARYING PLASMA POWERS, AND (d) DECONVOLUTED Si–CH_3 PEAK AT 20 W.

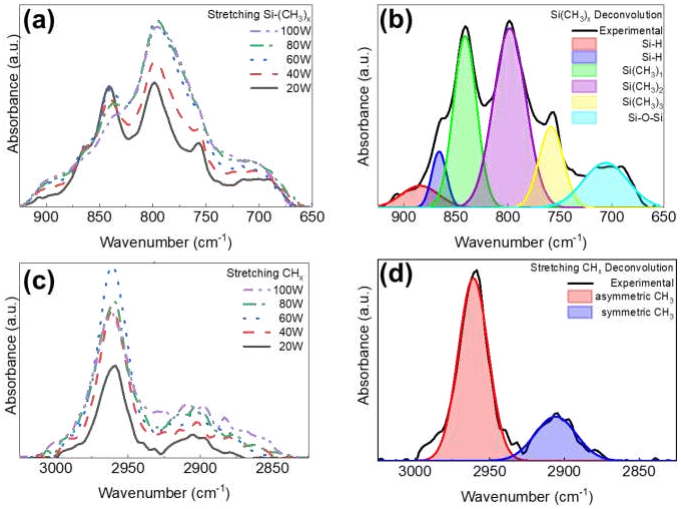

FIGURE 4: (a) FTIR ABSORPTION BAND OF Si–$(CH_3)_x$ (650-950 CM^{-1}) OF FILMS ON Si SUBSTATE AT VARYING PLASMA POWERS, (b) DECONVOLUTED Si–$(CH_3)_x$ PEAK AT 20 W PLASMA POWER, (c) FTIR ABSORPTION BAND OF C–H_x (3000-2800 CM^{-1}) AT VARYING PLASMA POWERS, AND (d) DECONVOLUTED C–H_x PEAK AT 20 W.

Figures 5(a)-(d) represent peak area ratios for deconvoluted absorption peaks of Si–O–Si stretching, Si–CH_3 bending, Si–$(CH_3)_x$ stretching, and CH_x stretching modes, respectively. As shown in Figure 5(a), the cage structure became dominant, and its peak area ratio increased from 10.8 to 67.4 % as the plasma power increased from 20 to 100 W. In comparison, the peak area ratio of network structure decreased from 82.4 to 26.4 % as the plasma power increased from 20 to 100 W.

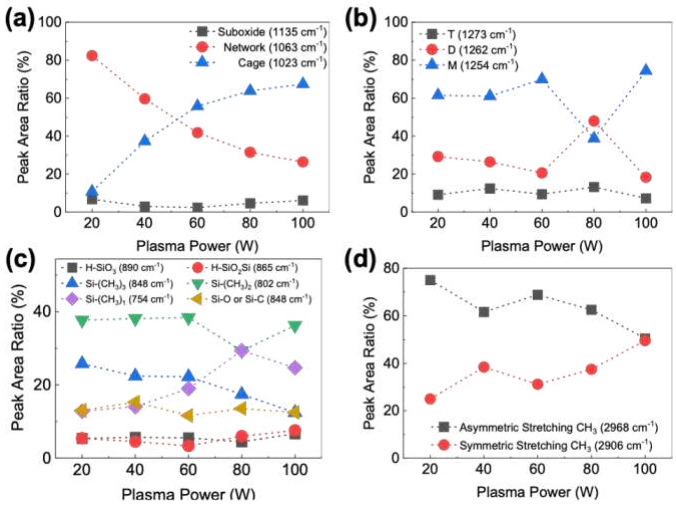

FIGURE 5: PEAK AREA RATIOS FOR DECONVOLUTED ABSORPTION PEAKS OF (a) Si–O–Si STRETCHING, (b) Si–CH_3 BENDING, (c) Si–$(CH_3)_x$ STRETCHING, AND (d) CH_x STRETCHING MODES.

The suboxidized structure showed the small peak area ratio below 6.8 %. It was known that the fraction of the cage structure in the CDO film strongly influences on the dielectric constant as well as porosity [18,21]. Thus, the fraction ratio between the cage and network structures could be related to the electrical and mechanical properties of the CDO thin films. Figure 5(b) shows that M-group was dominant with the peak area ratios above 61.1 % for all plasma powers except for 80 W, followed by D-group and T-group. In Figure 5(c), the Si–$(CH_3)_2$ peak was dominant with the peak area ratios of 29.3-38.4 % for all plasma powers. Notably, the peak area ratios of Si–$(CH_3)_3$ decreased from 25.8 to 12.4 % and those of Si–$(CH_3)_1$ increased from 12.8 to 24.7 % as the plasma power increased from 20 to 100 W. The peak area ratios of Si–O or Si–C maintained almost the same as 11.6-15.3 % for all plasma powers. Both H–SiO_3 and H–SiO_2Si peaks had relatively smaller peak area ratios below 7.6 % for all plasma powers. In Figure 5(d), the peak area ratios of asymmetric CH_3 stretching decreased from 75.0 to 50.5 % and those of symmetric CH_3 stretching increased from 25.0 to 49.5 % when the plasma power increased from 20 to 100 W.

High-resolution XPS scans were used to study the chemical bonding and elemental composition of the CDO thin films. Figure 6 shows the survey scan in the range of 0-1200 eV for varying plasma powers of 20-100 W. The three major peaks shown were Si2p (~284.8 eV), C1s (~102 eV), and O1s (~533 eV). Atomic concentrations of Si, C, and O were calculated for the five samples shown in Figure 7. For the TTMSS precursor itself, the atomic concentrations of Si, C, and O were 24, 57, and 19 %, respectively, which were derived from the chemical formula. As plasma power increased from 20 to 100 W, the carbon atomic concentration decreased from 41.9 to 39.0 %, whereas the oxygen atomic concentration increased from 19.8 to 21.8 %. The silicon atomic concentration was changed in the range of 38.3-39.2 %. In comparison to the contents of precursor itself, relatively smaller amount of carbon and higher amount of silicon were obtained without much change in the oxygen contents. This could be caused by the variation of plasma power level effecting the degree of the dissociation of TTMSS precursor in the plasma during the deposition. As a result, atomic composition within the CDO thin films can be controlled by varying the plasma powers during deposition. It should be noted that the carbon contents could be involved in the formation of the methyl functional groups of the CDO films.

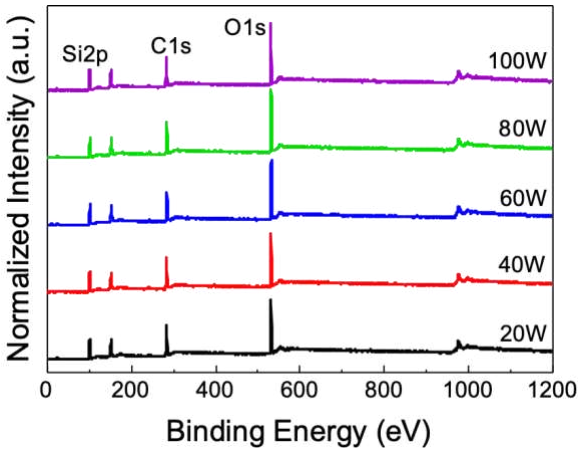

FIGURE 6: HIGH RESULTION XPS SURVEY SCAN OF CDO THIN FILMS ON Si SUBSTATE FOR VARYING PLASMA POWERS.

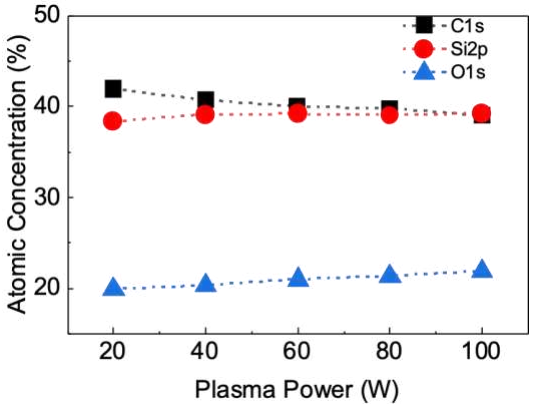

FIGURE 7: RELATIVE ATOMIC CONCENTRATION OF THE ELEMENTS IN THE CDO FILMS AT DIFFERENT PLASMA POWERS.

Figures 8(a) and (b) represent the Si2p peak in the XPS spectra of the CDO thin films for various plasma powers of 20-100 W and the deconvoluted peaks of Si2p for the power of 20 W, respectively. Three Gaussian peaks were deconvoluted into a D-group (~101 eV) designating an O_2–Si–C_2, a T-group (~102 eV) designating a O_3–Si–C, and an M-group (~103 eV) designating an O–Si–C_3 configurations [14,22].

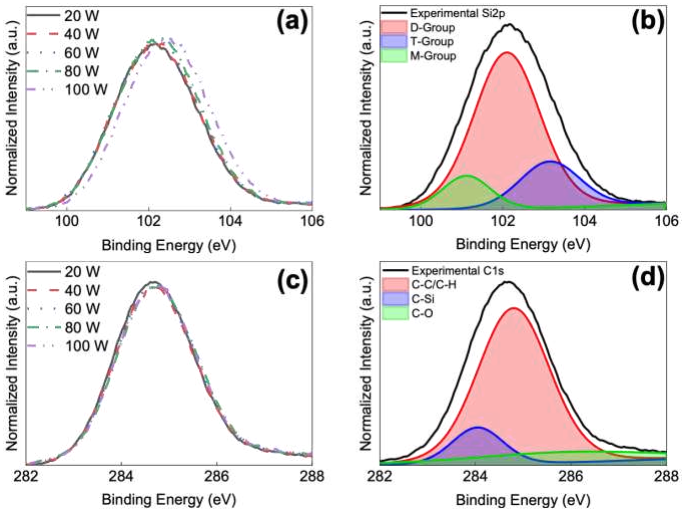

FIGURE 8: XPS SPECTRA OF (a) Si2p FOR THE FILMS AT VARYING PLASMA POWERS, (b) DECONVOLUTION OF THE Si2p PEAK AT 20 W, (c) C1s FOR THE FILMS AT VARYING PLASMA POWERS, AND (d) DECONVOLUTION OF THE C1s PEAK AT 20 W.

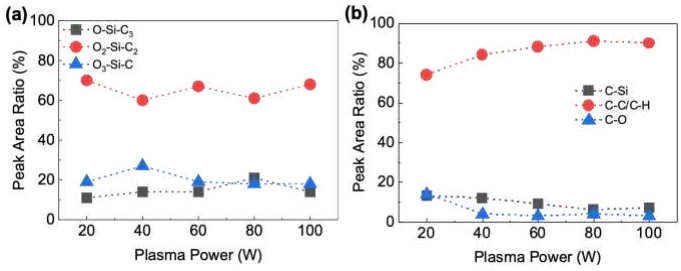

FIGURE 9: PEAK AREA RATIOS OF DECONVOLUTED (a) Si2p AND (b) C1s PEAKS AT VARYING PLASMA POWERS.

These configurations showed different binding energies determined by the numbers of carbon and oxygen atoms linked with a single silicon atom. The Q-group assigned to Si–O_4 (~104 eV) configuration, which comprises a fully oxidized silicon atom, did not appear for all samples [14,22]. It has been reported that the M-group forms a single oxygen linkage within the matrix, resulting in the termination of chain or network structures [23]. The D-group has two possible linkages through oxygen to the matrix without the formation of network and the T-group has three oxygen substituents causing easy formation of network [23]. The degree of network structure is known to be indicator to interpret mechanical strength of the CDO thin films [14,23]. Figures 8(c) and (d) show the C1s peak in the XPS spectra of the CDO thin films plotted for various plasma powers of 20-100 W and the deconvolution peaks of C1s for the power of 20 W. Each peak was deconvoluted into C–C/C–H (284.8 eV), C–Si (~284 eV), and C–O (~287 eV) configurations [14,22].

Figures 9(a) and (b) present peak area ratios for deconvoluted Si2p and C1s peaks of the CDO thin films for various plasma powers of 20-100 W, respectively. The D-group dominated by peak area ratios fluctuating between 60-70 % for all samples. In comparison, the peak area ratios of T- and M-groups were in the range of 18-27 and 11-21 %, respectively. The C–C/C–H were the dominant configuration of the C1s peak increasing from 74 to 90 % as the plasma power increased from 20 to 100 W. Other configurations of C–Si and C–O showed their peak area ratios below 20 %.

Although the deposition rates of the CDO thin films are not shown, they increased from 17.8 to 27.5 nm/min with increasing the plasma power from 20 to 100 W. In the deposition of the CDO thin films, two processes occur simultaneously: ablation that removes surface molecules and polymerization that deposits the surface monomer. These two processes are in competition. From the fact that the deposition rates increased as the plasma power increased, it was likely that the polymerization process was more dominant than the ablation process.

3.2 CDO Thin Films Deposited on ITO/PEN Substates

Like the analyses of the CDO thin films deposited on the Si substates, FTIR and XPS were used to study the chemical structures of the CDO thin films on ITO/PEN substrates at varying plasma powers. FTIR spectra scans from 4000 to 600 cm^{-1} were conducted for each sample and plotted in Figure 10. Each of the four prominent peaks present in the Si substate spectra scan were present in the ITO/PEN samples. The peaks of Si–O–Si stretching, Si–CH_3 bending, Si–$(CH_3)_x$ stretching, and CH_x stretching modes were assigned at 1200-900, 1300-1200, 950-650, and 3000-2800 cm^{-1}, respectively [13].

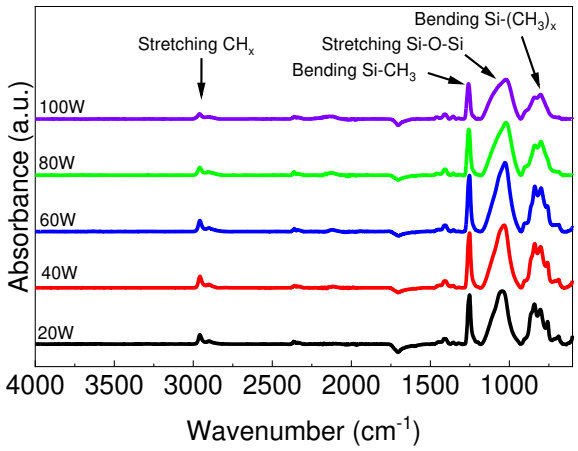

FIGURE 10: FTIR SPECTRA OF CDO THIN FILMS ON ITO/PEN SUBSTRATE AT VARYING PLASMA POWERS.

The peak intensities of Si–CH_3 and CH_x for the CDO thin films on ITO/PEN substrates showed higher than those for the films on Si substrates. During the deposition in the plasma, the surface reaction of the Si–O precursor with the silicon surface could lead the initial formation of Si–O bonds, resulting in favorable Si–O network formation. For the ITO/PEN substrates, the deficiency of silicon atoms on the ITO surface could be a barrier in the initial growth of Si–O structure. Thus, more hydrocarbon-related structures were observed in the CDO films deposited on ITO/PEN substrates.

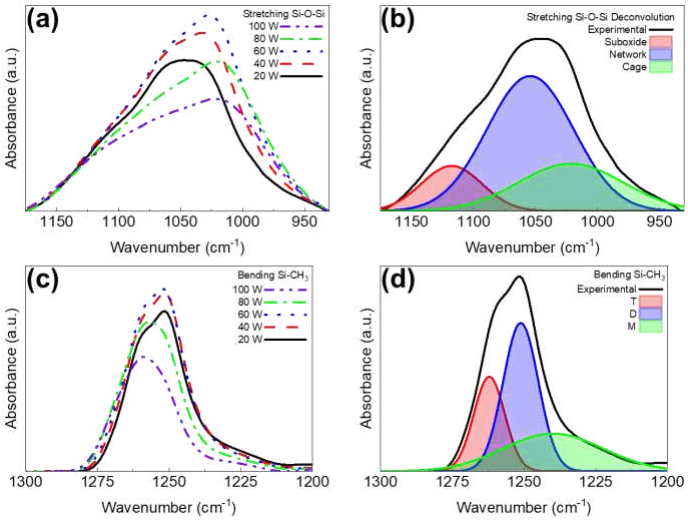

FIGURE 11: (a) FTIR ABSORPTION BAND OF Si–O–Si (900-1200 CM^{-1}) OF CDO FILMS ON ITO/PEN SUBSTATE AT VARYING PLASMA POWERS, (b) DECONVOLUTED Si–O–Si PEAK AT 20 W, (c) FTIR ABSORPTION BAND OF Si–CH_3 (1225-1300 CM^{-1}) AT VARYING PLASMA POWERS, AND (d) DECONVOLUTED Si–CH_3 PEAK AT 20 W.

Figures 11(a) and (b) present Si–O–Si stretching modes between 1200-900 cm^{-1} plotted at varying plasma powers of 20-100 W and its deconvoluted peaks at the plasma power of 20 W, respectively. As the plasma power increased from 20 to 60 W, the peak intensity of Si–O–Si increased. Then, the intensity of Si–O–Si decreased and the shape of it became collapsed as the plasma power increased from 60 to 100 W. The peaks were deconvoluted into three components corresponding to cage (1023 cm^{-1}), network (1063 cm^{-1}), and suboxide (1135 cm^{-1}) bonding configurations [18-20]. In Figure 11(c), FTIR spectra for Si–CH_3 bending modes between 1300-1200 cm^{-1} were plotted at varying plasma powers of 20-100 W and deconvoluted as shown for the plasma power of 20 W in Figure 11(d). As the plasma power increased from 20 to 60 W, the peak intensity of Si–CH_3 increased and then decreased below the intensity for 20 W with an increase of the plasma power to 100 W. Si–CH_3 peaks were deconvoluted into an M-group (1254 cm^{-1}), D-group (1262 cm^{-1}), and T-group (1273 cm^{-1}), corresponding to OSi–$(CH_3)_3$, O_2Si–$(CH_3)_2$, and O_3Si–CH_3, respectively.

Figures 12(a) and (b) show Si–$(CH_3)_x$ stretching modes between 950 and 650 cm^{-1} at varying plasma powers of 20-100 W and its deconvoluted peaks at the plasma power of 20 W, respectively. The peaks were allocated to H–SiO_3, H–SiO_2Si, Si$(CH_3)_1$, Si$(CH_3)_2$, Si$(CH_3)_3$, and Si–O–Si bonding. Figures 12(c) and (d) present CH_x stretching modes between 3000-2800 cm^{-1} plotted for varying plasma powers of 20-100 W and its deconvoluted peaks at the plasma power of 20 W, respectively. The CH_x peaks were deconvoluted into two peaks corresponding to asymmetric CH_3 and symmetric CH_3 bonding. There were some changes in the peak area ratios of these four absorption bands when the ITO/PEN substrates were used instead of Si substrates.

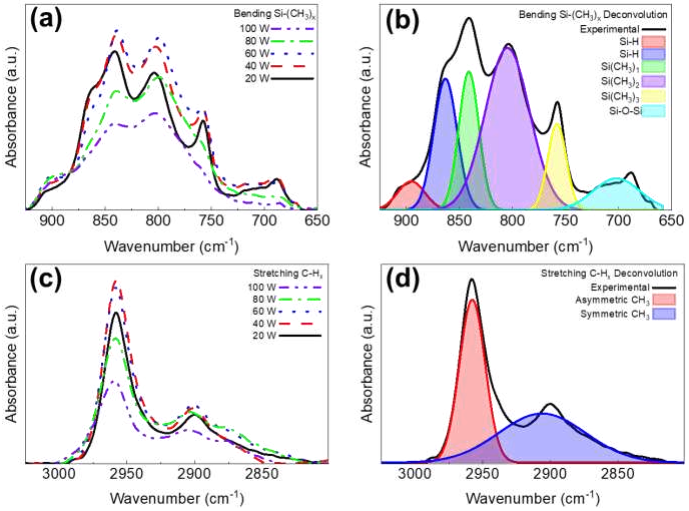

FIGURE 12: (a) FTIR ABSORPTION BAND OF Si–$(CH_3)_x$ (650-950 CM^{-1}) OF CDO FILMS ON ITO/PEN SUBSTATE AT VARYING PLASMA POWERS, (b) DECONVOLUTED Si–$(CH_3)_x$ PEAK AT 20 W, (c) FTIR ABSORPTION BAND OF C–H_x (3000-2800 CM^{-1}) AT VARYING PLASMA POWERS, AND (d) DECONVOLUTED C–H_x PEAK AT 20 W.

Figures 13(a)-(d) represent peak area ratios for deconvoluted absorption peaks of Si–O–Si stretching, Si–CH_3 bending, Si–$(CH_3)_x$ stretching, and CH_x stretching modes, respectively. As shown in Figure 13(a), the cage structure was still dominant except for the case of 20 W and its peak area ratio increased from 25.5 to 75.8 % as the plasma power increased from 20 to 60 W and the ratio decreased to 56.9 % for the power of 100 W. In comparison, the peak area ratio of network structure decreased from 60.3 to 8.6 % as the plasma power increased from 20 to 60 W and the ratio increased to 24.9 % for the power of 100 W. The suboxidized structure showed the small peak area ratio below 18.2 %. Figure 13(b) shows that the highest peak area ratio (78.3 %) of T-group and the lowest peak area ratio (4.5 %) of D-group were obtained for the plasma power of 60 W. The peak area ratio of M-group decreased from 31.5 to 6.8 % when the plasma power increased from 20 to 100 W.

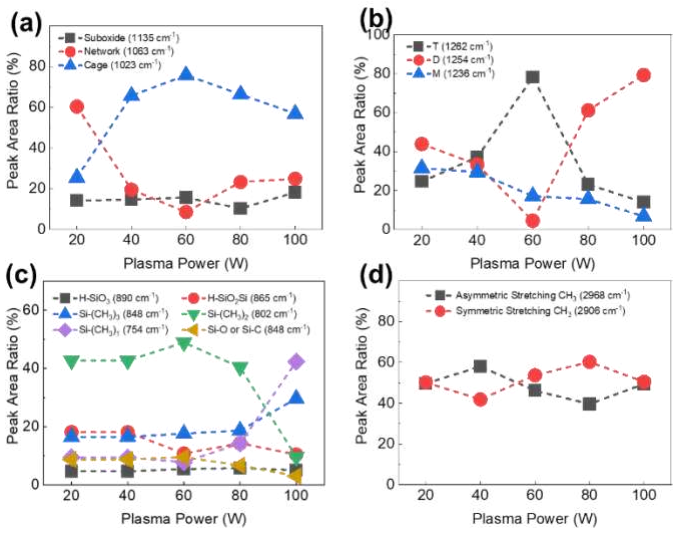

FIGURE 13: PEAK AREA RATIOS OF CDO FILMS ON ITO/PEN SUBSTRATE FOR DECONVOLUTED ABSORPTION PEAKS OF (a) Si–O–Si STRETCHING, (b) Si–CH_3 BENDING, (c) Si–$(CH_3)_x$ STRETCHING, AND (d) CH_x STRETCHING.

In Figure 13(c), the Si–$(CH_3)_2$ peak was still dominant with the peak area ratios above 40.4 % except for the case of 100 W. The peak area ratios of Si–$(CH_3)_3$ increased from 16.5 to 29.6 %, those of Si–$(CH_3)_1$ increased from 9.4 to 42.3 %, and those of H–SiO_2Si decreased from 18.1 to 10.4 % as the plasma power increased from 20 to 100 W. Both peak area ratios of Si–O or Si–C and H–SiO_3 maintained below 9.5 % for all plasma powers. In Figure 13(d), the peak area ratios of asymmetric and symmetric CH_3 stretching modes did not show the tendency dependent on the plasma power.

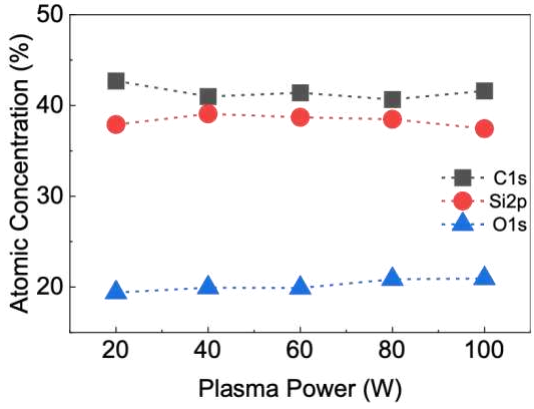

FIGURE 14: RELATIVE ATOMIC CONCENTRATION OF THE ELEMENTS IN THE CDO FILMS ON ITO/PEN SUBSTRATES AT DIFFERENT PLASMA POWERS.

XPS analysis was performed on the CDO thin films on ITO/PEN substrates for various plasma powers of 20-100 W using the same process as shown above for Si substate samples. Very similar survey scans for the CDO thin films on ITO/PEN substrates to those for Si substrates were obtained in the range of 0-1200 eV. Figure 14 shows the atomic concentrations of Si, C, and O calculated from three major peaks of Si2p (~284.8 eV), C1s (~102 eV), and O1s (~533 eV). The carbon and silicon atomic concentrations were in the range of 40.7-42.7 and 37.5-39.1 % for the plasma powers of 20-100 W, respectively. The oxygen atomic concentration increased from 19.4% to 20.9 %. More carbon and less silicon and oxygen contents in the CDO films on ITO/PEN substrates were obtained than those on the Si substrates. It is consistent with the fact that more hydrocarbon-related structures were observed from the FTIR analysis.

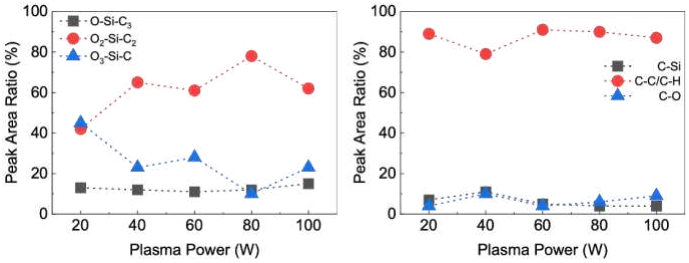

FIGURE 15: PEAK AREA RATIOS OF DECONVOLUTED (a) Si2p AND (b) C1s PEAKS AT VARYING PLASMA POWERS.

Figures 15(a) and (b) present peak area ratios for deconvoluted Si2p and C1s peaks of the CDO thin films for various plasma powers of 20-100 W, respectively. The D-group (O_2–Si–C_2) was dominant, and its peak area ratio increased from 42 to 78 % as the plasma power increased from 20 to 80 W and it decreased to 62 % for the plasma power of 100 W. The peak area ratio of T-group (O_3–Si–C) decreased from 45 to 23 % as the plasma power increased from 20 to 100 W. The peak area ratio of M-group (O–Si–C_3) remained in the range of 11-15 %. As shown in the CDO films on Si substrates, the C–C/C–H were main configuration of the C1s peak in the range of 79-91 %. Other configurations of C–Si and C–O showed their peak area ratios below 11 %.

4. CONCLUSION

The CDO thin films as low dielectric constant materials were deposited on both n-type Si and ITO/PEN substrates, using the PECVD of TTMSS precursor. The prominent peaks from the FTIR spectra included Si–O–Si stretching, Si–CH_3 bending, Si–$(CH_3)_x$ stretching, and CH_x stretching modes. The peak area ratios of deconvoluted peaks for each absorption band depended on the substrate type. For the Si-O-Si stretching mode, the fraction of the cage structure increased and the fraction of the network structure decreased with increased plasma power for the CDO films on Si substate. For the ITO/PEN substrate, the fraction of the cage structure increased before decreasing after 60 W and the fraction of the network structure decreased before increasing at 60 W. The CDO films on Si substate had a lower suboxide fraction than that of ITO/PEN. From XPS analysis, it was found that for CDO films on both Si and ITO/PEN substates, O_2-Si-C_2 and C-C/C-H were the prominent bonding structures for the Si2p and C1s peaks, respectively. Additionally, it was

observed that CDO thin films on ITO/PEN had a higher carbon concentration than the Si samples. The chemical structures will be strongly related to electrical and mechanical performance of the CDO films.

ACKNOWLEDGEMENTS

This work was jointly supported by NSF Civil, Mechanical and Manufacturing Innovation Division (CMMI) and the Established Program to Stimulate Competitive Research (EPSCoR).

REFERENCES

[1] R.H. Havemann, J.A. Hutchby, *Proc. IEE*E 89 (2001) 586–601.
[2] S. List, M. Bamal, M. Stucchi, K. Maex, *Microelectron. Eng*. 83 (2006) 2200–2207.
[3] M. Baklanov, K. Maex, M. Green, *Wiley & Sons*, New Jersey, 2007.
[4] K. Maex, M.R. Baklanov, D. Shamiryan, F. Lacopi, S.H. Brongersma, Z. S. Yanovitskaya, *J. Appl. Phys*. 93 (2003) 8793–8841.
[5] W. Volksen, R.D. Miller, G. Dubois, *Chem. Rev*. 110 (2009) 56–110.
[6] A. Grill, V. Patel, *Appl. Phys. Lett*. 79 (2001) 803–805.
[7] L. Favennec, V. Jousseaume, G. Gerbaud, A. Zenasni, G. Passemard, *J. Appl. Phys*. 102 (2007) 064107-1–064107-9.
[8] A.M. Urbanowicz, K. Vanstreels, P. Verdonck, D. Shamiryan, S. De Gendt, M. R. Baklanov, *J. Appl. Phys*. 107 (2010) 104122-1-104122-7.
[9] A. Grill, *Annu. Rev. Mater. Res*. 39 (2009) 49–69.
[10] D. Kim, H. Kim, H. Jang, D. Jung, H. Chae, *J. Nanosci. Nanotechnol*. 12(7) (2012) 6040–6044.
[11] P. Verdonck, C. Wang, Q.T. Le, L. Souriau, K. Vanstreels, M. Krishtab, M. Baklanov, *Microelectron. Eng*. 120 (2014) 225–229.
[12] H. Kim, H. Oh, C. Lee, D. Jung, J. Boo, *Bull. Korean Chem. Soc*. 35(10) (2014) 2941–2944.
[13] Y. Lee, W. Ban, S. Jang, D. Jung, *J. Nanosci. Nanotechnol.* 21 (2021) 2139–2147.
[14] Y. Park, H. Lim, S. Kwon, W. Ban, S. Jang, D. Jung, *Thin Solid Films* 727 (2021) 138680.
[15] M.R. Baklanov, K.P. Mogilnikov, *Microelectron. Eng*. 64 (2002) 335–349.
[16] H. You, P. Mennell, M. Shoudy, D. Sil, D. Dorman, S. Cohen, E. Liniger, T. Shaw, T. L. Leo, D. Canaperi, M. Raymond, A. Madan, A. Grill, *J. Vac. Sci. Technol. B Nanotechnol. Microelectron*. 36 (2018) 012202-1–012202-8.
[17] A. Grill, *J. Appl. Phys*. 93 (2003) 1785–1790.
[18] A. Grill, D.A Neumayer, *J. Appl. Phys*. 94 (2003) 6697–6707.
[19] S.C. Deshmukh, E.S. Aydil, *J. Vac. Sci. Technol*. A 13 (1995) 2355–2367.
[20] Y. Kikuchi, A. Wada, T. Kurotori, M. Sakamoto, T. Nozawa, S. Samukawa, *J. Phys. D* 46 (2013) 395203(1)–395203(7).
[21] S. Kwon, W. Ban, H. Kim, Y. Park, Y. Kim, S. Yu, D. Jung, *Sci. Adv. Mater*. 10 (2018) 1147–1153.
[22] Z.J. Ding, Y.P. Wang, W.J. Liu, S.J. Ding, M.R. Baklanov, D.W. Zhang, *J. Phys. D Appl. Phys*. 51 (2018) 115103(1)–115103(7).
[23] D.D. Burkey, K.K. Gleason, *J. Electrochem. Soc*. 151 (2004) F105–F112.